Available online at www.sciencedirect.com

SCIENCE DIRECT®

Coastal Engineering 52 (2005) 391–407

Coastal Engineering
An International Journal for Coastal, Harbour and Offshore Engineers

www.elsevier.com/locate/coastaleng

Numerical implementation of the harmonic modified mild-slope equation

Rodolfo Silva[a,*], Alistair G.L. Borthwick[b,1], Rodney Eatock Taylor[b,1]

[a]Instituto de Ingeniería-UNAM, Cd. Universitaria, Apdo. Postal 70-472, 04510 D.F., México
[b]Department of Engineering Science, University of Oxford, Oxford OX1 3PJ, UK

Received 10 April 2003; received in revised form 2 November 2004; accepted 10 December 2004
Available online 29 March 2005

Abstract

A numerical solver is presented of the modified time-independent mild-slope equation, which incorporates energy dissipation. Using a second-order parabolic approximation, the following external boundary conditions are modelled: open and fully transmitting to both incoming and outgoing waves; partially reflecting, and; fully absorbing. Discretisation of the governing equation and boundary conditions is by means of a second-order accurate central difference scheme. The resulting sparse-banded matrix is solved using an inexpensive banded solver with Gaussian elimination. The numerical predictions are in excellent agreement with the analytical solution for the interaction of non-breaking waves with an array of vertical surface-piercing circular cylinders on a horizontal bed. Results are compared with those for the same array on various seabed topographies. The model is robust and can be used for wave propagation in complex geometries. It has fewer restrictions associated with wave obliqueness at boundaries than traditional models based on the mild-slope equation.

Keywords: Mild-slope equation; Finite differences; Gaussian elimination; Radiation condition; Maximum directional aperture

1. Introduction

Accurate prediction of water wave transformation over an irregular bed topography on which structures may be sited is important to engineers who plan, design, construct, and maintain coastal facilities. When a wave train propagates from deep to shallow water several transformations take place, such as shoaling, refraction, reflection, diffraction, resonance, and energy dissipation induced by bottom friction, turbulence and wave breaking. Various theoretical approximations have been derived in recent decades, under the assumption of linear wave theory. One way to model these kinds of phenomena is through the well-known mild-slope equation.

The basic mild-slope equation provides a means of estimating the transformation of linear waves in water over a slowly varying impermeable bottom, and was

* Corresponding author. Fax: +52 55 5616 2164.
E-mail addresses: RSilvaC@iingen.unam.mx (R. Silva), alistair.borthwick@eng.ox.ac.uk (A.G.L. Borthwick), r.eatocktaylor@eng.ox.ac.uk (R.E. Taylor).
[1] Fax: +44 1865 273010.

0378-3839/$ - see front matter © 2005 Elsevier B.V. All rights reserved.
doi:10.1016/j.coastaleng.2004.12.009

originally derived by Berkhoff (1972) and Smith and Sprinks (1975). Although various studies have attempted to apply the mild-slope equation to wave propagation over steeply varying impermeable bed topographies, Booij (1983) proved that the mild-slope solution is formally only valid for slopes of 1:3 or less. Massel (1993) presented a mild-slope approximation, which includes the effect of evanescent modes. Chamberlain and Porter (1995) derived a modified version of the mild-slope equation that retains second-order terms, and Porter and Staziker (1995) derived a solution that takes into account the terms associated with the evanescent modes with depth-averaged mass flux and pressure boundary conditions for the case of unidirectional wave transformation.

Following Maa et al. (2002), numerical solvers of the mild-slope equation are based on:

(1) The parabolic approximation, which is only valid when reflection is negligible and wave diffraction is weak (e.g. Kirby and Dalrymple, 1994).
(2) The hyperbolic approach, whereby the elliptic equation is converted to a pair of transient relations (e.g. Copeland, 1985; Suh et al., 1997), offers the advantage of reduced computing time compared with alternative elliptic solvers, such as the alternating direction implicit (ADI) algorithm (e.g. Madsen and Larsen, 1987) and the conjugate gradient method (e.g. Panchang et al., 1991).
(3) An iterative approach for solving the elliptic equation, which normally does not require a large amount of computer memory and has a rapid convergence rate, but can be unstable and involves complicated computer algorithms making program maintenance difficult (e.g. Oliveira and Anastasiou, 1998).
(4) Direct matrix equation solvers, which are sufficiently robust to handle very complex configurations (e.g. Maa et al., 1997).

When solving the extended mild-slope equation, Maa et al. (2002) implemented a special book-keeping procedure for Gaussian elimination with partial pivoting that transforms the (large) memory requirements from core to hard disk. The method is direct and computationally economical. However, the solution presented by Maa et al. (2002) includes the lowest parabolic approximation for the open boundaries and consequently is only valid when the angle of approach of the wave to the boundaries is less than 30°, and so only partially reflecting lateral boundaries are allowed.

The mathematical model used here is based on the modified version of the harmonic mild-slope equation derived by Chamberlain and Porter (1995). To take into account energy losses from breaking and bottom friction, the modified mild-slope equation is altered to incorporate an energy dissipation term, in a similar way to Kirby and Dalrymple (1994) and Dingemans (1997). Boundaries are assumed to be either open (fully transmitting to both incoming and outgoing waves), or partially reflecting, or fully absorbing through the second-order parabolic approximation, Kirby (1989). A central difference technique of second-order accuracy is used to discretise the governing equation. Limitations of the present model are: its linear character; neglect of evanescent modes; numerical restrictions intrinsic to the finite difference technique; and artificial absorption or reflection into the numerical domain introduced by the approximation used for the open and partially transmissive boundary.

To the best of the authors' knowledge, it is the first time that the steady-state modified mild-slope equation has been solved using a finite difference scheme together with a second-order parabolic approximation to represent the external boundary conditions. In all cases, the numerical predictions are in excellent agreement with analytical solutions. The model has fewer restrictions associated with wave obliqueness at boundaries than traditional models based on the mild-slope equation.

Although the present model is applicable to totally reflective lateral boundaries, such cases are not considered herein. This is because the present model reduces to that of Maa et al. (2002) for reflective boundaries, which has previously been validated.

2. Theoretical background

Consider a homogeneous incompressible fluid with irrotational motion travelling over an impermeable bottom with spatially varying water depth $h(x,y)$. For the three-dimensional problem, the governing equation is derived from the continuity equation and can be expressed (see, e.g. Dingemans, 1997) in terms of the velocity potential Φ, as:

$$\nabla_h^2\Phi + \frac{\partial^2\Phi}{\partial z^2} = 0 \quad -h(x,y)\le z\le 0, \tag{1}$$

where (x,y) represents the horizontal coordinates, z is the vertical coordinate measured positively upwards with the undisturbed free surface at $z=0$, and $\nabla_h=(\partial/\partial x,\partial/\partial y)$ is the horizontal gradient operator.

The mixed free surface boundary condition, obtained by combining the linear dynamic and kinematic free surface boundary conditions for variable depth, is:

$$g\frac{\partial\Phi}{\partial z} + \frac{\partial^2\Phi}{\partial t^2} = 0; \quad z=0. \tag{2}$$

The kinematic boundary condition at the impermeable bottom, $z=-sh$ is

$$\frac{\partial\Phi}{\partial z} + \nabla_h h\cdot\nabla_h\Phi = 0 \quad z=-h(x,y) \tag{3}$$

where t is time and g is acceleration due to gravity.

The velocity potential Φ can be expressed as:

$$\Phi(x,y,z,t) = Re\{\varphi(x,y,t)f(z)\}, \tag{4}$$

where Re is the real part of the argument and φ is the complex amplitude of the water surface. The depth dependency, corresponding to a horizontal bottom $\nabla_h h=0$, is provided by

$$f(z) = \frac{\cosh k(h+z)}{\cosh kh}. \tag{5}$$

The wavenumber k is determined from

$$\frac{\sigma^2 h}{g} = kh\tanh kh, \tag{6}$$

where σ is the angular frequency ($\sigma=2\pi/T$) and T is the wave period.

Following Smith and Sprinks (1975), application of Green's second identity to $f(z)$ and Φ gives

$$\int_{-h}^{0} f\frac{\partial^2\Phi}{\partial z^2}dz - \int_{-h}^{0}\Phi\frac{\partial^2 f}{\partial z^2}dz - \left[f\frac{\partial\Phi}{\partial z} - \Phi\frac{\partial f}{\partial z}\right]_{-h}^{0} = 0 \tag{7}$$

Substituting Eqs. (1) and (4) in the first term of Eq. (7), Eqs. (4) and (5) in the second term of Eq. (7) and Eqs. (2) and (3) in the last term of Eq. (7), the modified time-dependent mild-slope equation is obtained as:

$$\nabla_h(I_1\nabla\varphi) + k^2\varphi I_1 + \varphi r(h) = \frac{1}{g}\frac{\partial^2\varphi}{\partial t^2} + \varphi\frac{\sigma^2}{g}, \tag{8}$$

where

$$r(h) = I_2\nabla_h^2 h + (\nabla_h h)^2\left(\frac{\partial I_2}{\partial h} - I_3\right), \tag{9}$$

$$I_1 = \int_{-h}^{0} f^2 dz, \tag{10}$$

$$I_2 = \int_{-h}^{0} f\frac{\partial f}{\partial h}dz, \tag{11}$$

and

$$I_3 = \int_{-h}^{0}\left(\frac{\partial f}{\partial h}\right)^2 dz. \tag{12}$$

To obtain the time-independent version of the mild-slope equation, the velocity potential is written in separated form as:

$$\varphi(x,y,t) = \phi(x,y)e^{-i\sigma t}. \tag{13}$$

Finally, substituting Eq. (13) into Eq. (8), the modified time-independent mild-slope equation is expressed.

$$\nabla_h(I_1\nabla\phi) + k^2\phi I_1 + \phi r(h) = 0. \tag{14}$$

It should be noted that Chamberlain and Porter (1995) derived Eq. (14) using Hamilton's variational principle.

In a similar way to Dingemans (1997), Eq. (14) is modified to incorporate an energy dissipation term, which takes into account dissipation due to wave breaking and bottom friction,

$$\nabla_h\cdot I_1\nabla_h\phi + \left[\left(k^2 + i\sigma D\right)I_1 + r(h)\right]\phi = 0, \tag{15}$$

where D is the dissipation factor. In this paper, only wave breaking and bottom friction dissipation are considered, and so

$$D = f_D + f_B. \tag{16}$$

The breaking dissipation factor, f_D, may be expressed (Dally et al., 1985):

$$f_D = \frac{kC_k}{\sigma h}\left[1-\left(\frac{C_G h}{H_B}\right)^2\right], \tag{17}$$

where H_B is the wave height at the breaking point, (easily evaluated through $H_B=\gamma h$, with $\gamma=0.8$), $C_k=0.15$, and $C_G=0.4$.

In practice, the wave-induced bottom boundary layer is usually turbulent. The dissipation term is given by (Kirby and Dalrymple, 1994),

$$f_B = \frac{4}{3\pi}\frac{C_f a\sigma^2}{ng\sinh^3 kh}, \tag{18}$$

where C_f is the Darcy–Weisbach friction factor, a is the local wave amplitude ($H/2$), σ is the angular frequency and

$$n = \frac{1}{2}\left(1+\frac{2kh}{\sinh 2kh}\right). \tag{19}$$

3. Numerical implementation

Without loss of generality, the modified time-independent mild-slope equation, Eq. (15) can be written in its Helmholtz form (Radder, 1979) as

$$\nabla_h^2\psi + K_c^2\psi = 0, \tag{20}$$

where,

$$\psi = (I_1)^{1/2}\phi, \tag{21}$$

and

$$K_c^2 = \left(k^2 + i\sigma D\right) + \frac{r(h)}{I_1} - \frac{\nabla^2\sqrt{I_1}}{\sqrt{I_1}}. \tag{22}$$

To solve Eq. (20) a numerical scheme with appropriate boundary conditions has to be implemented. Two types of boundary conditions are considered herein: (a) an open boundary; and (b) a partially reflecting boundary condition. The open boundary allows full transmission of both incoming and outgoing waves. At its extremes, the partially reflecting boundary condition tends to either a totally reflecting or a fully absorbing boundary condition.

For simplicity and convenience, the seaward boundary condition is treated as an open boundary of constant depth, the landward boundary as partially reflecting, and the lateral boundaries as open or partially reflecting. The exterior bathymetry varies only in the cross-shore direction, as shown in Fig. 1.

For the case of an open boundary condition, Kirby (1989) demonstrated the advantages to be gained by adopting the parabolic approximation as a radiation boundary condition for the finite difference solver. Following Dingemans (1997), an equivalent way of writing Helmholtz Eq. (20) is

$$\frac{\partial^2\psi}{\partial x^2} = -K_c^2\left(1+\frac{1}{K_c^2}\frac{\partial^2\psi}{\partial y^2}\right). \tag{23}$$

Propagation in the positive x-direction can be described by means of pseudo-differential operators as

$$\frac{\partial\psi}{\partial x} = iK_c\left(1+\frac{1}{K_c^2}\frac{\partial^2}{\partial y^2}\right)^{1/2}\psi. \tag{24}$$

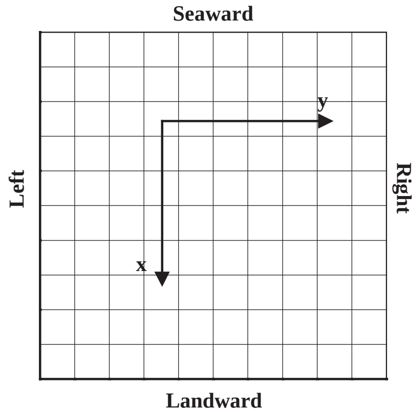

Fig. 1. Coordinate system and grid alignment for the computing domain.

A parabolic approximation of Eq. (24) can be obtained,

$$\frac{\partial\psi}{\partial x} = iK_c\left(a_0\psi + \frac{a_1}{K_c^2}\frac{\partial^2\psi}{\partial y^2}\right) - \frac{a_2}{K_c^2}\frac{\partial^3\psi}{\partial x\partial y^2}, \tag{25}$$

where the values of the parameters a_0, a_1 and a_2 depend on the maximum directional aperture and the degree to which the condition of exact transmission at normal incidence is met. The parameters can be estimated by means of a Padé approximant or the approximation given by Kirby (1986).

For the seaward boundary condition, the total potential is the sum of incident and scattered waves. Using Eq. (25) as an approximation for the scattered waves,

$$\frac{\partial\psi_s}{\partial x} = \frac{\partial(\psi-\psi_i)}{\partial x} = -iK_c\left(a_0(\psi-\psi_i) + \frac{a_1}{K_c^2}\frac{\partial^2(\psi-\psi_i)}{\partial y^2}\right) + \frac{a_2}{K_c^2}\frac{\partial^3(\psi-\psi_i)}{\partial x\partial y^2}. \tag{26}$$

In Eq. (26) the scattered waves travel towards the seaward boundary in directions that partially oppose the incident waves. Hence, the incident velocity potential is defined as

$$\psi^g = \frac{iHg}{2\sigma}\sqrt{I_1}\frac{\cos hk(h+z)}{\cos hkh}\exp[ik(x\cos\theta + y\sin\theta)]. \tag{27}$$

Substituting Eq. (27) into Eq. (26), we obtain

$$\begin{aligned}\frac{\partial\psi}{\partial x} &= -iK_c a_0\psi - i\frac{a_1}{K_c}\frac{\partial^2\psi}{\partial y^2} + \frac{a_2}{K_c^2}\frac{\partial^3\psi}{\partial x\partial y^2} + i\left(K_c a_0 - \frac{k^2 a_1\sin^2\theta}{K_c} + \frac{k^3 a_2\sin^2\theta\cos\theta}{K_c^2} + k\cos\theta\right)\psi_i \\ &\approx -\left(iK_c a_0\psi + i\frac{a_1}{K_c}\frac{\partial^2\psi}{\partial y^2} + \frac{a_2}{K_c^2}\frac{\partial^3\psi}{\partial x\partial y^2}\right) + i(k+K_c)\psi^g\cos\theta.\end{aligned} \tag{28}$$

An analogous procedure can be given for the y-direction, if it is assumed that the lateral boundaries have constant water depth and reflections from the landward side can be disregarded. In practice, however, the depth usually decreases in the landward direction. Moreover, the plane wave formulation does not include the effects of breaking. When this procedure is used in conjunction with the governing Eq. (20) in the interior of the domain with wave breaking, a discontinuity along the open boundary results from incorrect forcing. To overcome this limitation, it is therefore assumed that the depths at the lateral boundaries change solely in the x-direction (as also implemented by Zhao et al., 2001).

Under the assumption that the problem becomes one-dimensional at the lateral boundaries, the governing equation simplifies to give,

$$\frac{\partial^2\psi}{\partial x^2} + K_c^2\psi = 0. \tag{29}$$

At the offshore boundary, it is assumed that the total velocity potential ψ_1 is composed of the sum of incident and reflected waves,

$$\psi_1 = \psi^g + \psi^r. \tag{30}$$

The incident velocity potential is given by Eq. (27), and the reflected velocity potential may be expressed as

$$\psi^r = \frac{iHRg}{2\sigma}\sqrt{I_l}\frac{\cosh k(h+z)}{\cosh kh}\exp[-ik(x\cos\theta - y\sin\theta)], \tag{31}$$

where R is the reflection coefficient. Neglecting diffraction and dissipation effects, and assuming constant water depth at the seaward boundary, Eq. (28) simplifies to give

$$\frac{\partial\psi_1}{\partial x} = ik\cos\theta(2\psi_i - \psi). \tag{32}$$

The landward boundary condition is obtained using the assumption that the wave field may be decomposed into wave trains that approach and are reflected from the coast (Steward and Panchang, 2000),

$$\psi_l = A(\exp[ikx\cos\theta_l] + R\exp[-ik(x\cos\theta_l - \beta)]), \tag{33}$$

where A is the amplitude of the approaching waves, β is the phase shift, and θ_1 is the local angle at which approaching waves intersect the boundary. Evaluating the partial derivative in the x-direction,

$$\frac{\partial\psi_1}{\partial x} = ikA\cos\theta_1(\exp[ikx\cos\theta_1] - R\exp[-ik(x\cos\theta_1 - \beta)]). \tag{34}$$

Without loss of generality the x-coordinate is located at $x=0$, and after substituting Eqs. (27) and (31) into Eq. (30), the right-hand side of this equation can be multiplied by ψ_1 and divided by the expression for ψ_1, obtaining

$$\frac{\partial\psi_1}{\partial x} = ik\gamma_1\psi_1\cos\theta_1, \tag{35}$$

where

$$\gamma_1 = \frac{1 - R\exp[ik\beta]}{1 + R\exp[ik\beta]}. \tag{36}$$

The value of the phase shift β is difficult to determine, hence it is normally set as $\beta=0$. Assuming that it is valid to use Snell's law, the local angle θ_1 may be estimated from

$$\sin\theta_1 = \frac{k_0}{k_1}\sin\theta, \tag{37}$$

where k_0 is the wave number at the seaward boundary and k_1 is the local wave number at the location of interest.

The lateral boundary conditions can be established through the following equation,

$$\frac{\partial \psi}{\partial y} = \pm\left(iK_c a_0\psi + i\frac{a_1}{K_c}\frac{\partial^2\psi}{\partial x^2} + \frac{a_2}{K_c^2}\frac{\partial^3\psi}{\partial y\partial x^2}\right) + 2ik_1\psi_1\cos\theta_1, \text{ on } \pm y \text{ boundary.} \tag{38}$$

Since the breaking parameter and bottom friction dissipation term are functions of the local wave height and are unknown beforehand, Eq. (29) has to be solved by an iteration procedure. In the first iteration no dissipation term is considered, and the resulting velocity potential is used as the initial local incident velocity potential. In the second iteration the dissipation terms are evaluated using the local wave height, and so on.

For the case of a partially reflected boundary condition, consider a linear wave train travelling from the interior to the exterior of the domain. When this wave reaches the boundary it is partially reflected into the domain and partially transmitted outside the domain. Following the same procedure as that described above, the partially reflected boundary conditions can be expressed as:

$$\frac{\partial \psi}{\partial x} = \gamma\left[iK_c\left(a_0\psi + \frac{a_1}{K_c^2}\frac{\partial^2\psi}{\partial y^2}\right) - \frac{a_2}{K_c^2}\frac{\partial}{\partial x}\left(\frac{\partial^2\psi}{\partial y^2}\right)\right], \quad \text{on} + x \text{ boundary,} \tag{39}$$

and

$$\frac{\partial \psi}{\partial y} = \pm\gamma\left[iK_c\left(a_0\psi + \frac{a_1}{K_c^2}\frac{\partial^2\psi}{\partial x^2}\right) - \frac{a_2}{K_c^2}\frac{\partial}{\partial y}\left(\frac{\partial^2\psi}{\partial x^2}\right)\right], \quad \text{on } \pm y \text{ boundary.} \tag{40}$$

Eqs. (39) and (40) represent a total reflection boundary condition when $\gamma=0$, a radiation boundary condition when $\gamma=1$, and a partial boundary condition when $0<\gamma<1$.

Using second-order accurate central differences, the governing equation, Eq. (20), may be written in discretised form as:

$$\frac{\psi_{i,j-1} - 2\psi_{i,j} + \psi_{i,j+1}}{\Delta y^2} + \frac{\psi_{i-1,j} - 2\psi_{i,j} + \psi_{i+1,j}}{\Delta x^2} + K_c^2\psi_{i,j} = 0. \tag{41}$$

In order to obtain a second-order approximation to the boundary condition, it is necessary to consider a fictitious cell point located one grid increment outside the study domain. For example, using forward and central differences, the seaward boundary condition, Eq. (28), can be expressed as,

$$\begin{aligned}\frac{\left(\psi_{i+1,j} - \psi_{i-1,j}\right)}{2\Delta x} &= i(k+K_c)\psi^{g}\cos\theta - iK_c a_0\psi_{i,j} - i\frac{a_1}{K_c}\frac{\psi_{i,j+1} - 2\psi_{i,j} + \psi_{i,j-1}}{\Delta y^2} + \frac{a_2}{K_c^2}\\ &\times\frac{3\left(\psi_{i,j+1} - 2\psi_{i,j} + \psi_{i,j-1}\right) - 4\left(\psi_{i+1,j+1} - 2\psi_{i+1,j} + \psi_{i+1,j-1}\right) + \psi_{i+2,j+1} - 2\psi_{i+2,j} + \psi_{i+2,j-1}}{2\Delta x\Delta y^2}\end{aligned} \tag{42}$$

Using Eqs. (41) and (42) to eliminate $\psi_{i-1,j}$ at the fictitious point, the discretised boundary equation becomes,

$$\begin{aligned}&\left(i\frac{a_1}{K_c}2\Delta x - 3\frac{a_2}{K_c^2} + \Delta x^2\right)\psi_{i,j-1} - 2\left(\Delta y^2 + \Delta x^2 + \Delta y^2\Delta x^2K_c^2(1+2ia_0) - 2i\frac{a_1}{K_c}\Delta x + 3\frac{a_2}{K_c^2}\right)\psi_{i,j}\\ &+\left(i\frac{a_1}{K_c}2\Delta x - 3\frac{a_2}{K_c^2} + \Delta y^2 + \Delta x^2\right)\psi_{i,j+1} + 4\frac{a_2}{K_c^2}\psi_{i+1,j+1}\left(\Delta y^2 - 8\frac{a_2}{K_c^2}\right)\psi_{i+1,j} + 4\frac{a_2}{K_c^2}\psi_{i+1,j-1}\\ &+\frac{a_2}{K_c^2}\psi_{i+2,j+1} - 2\frac{a_2}{K_c^2}\psi_{i+2,j} + \frac{a_2}{K_c^2}\psi_{i+2,j-1} = 2\Delta x\Delta y^2 i(k+K_c)\psi^{g}\cos\theta\end{aligned} \tag{43}$$

At corner points of the grid, second-order finite difference expressions are derived from Eqs. (20), (28) and (38).

Eq. (41) and the boundary finite difference equations are applied to all water grid points in the domain. The resulting banded matrix equation is solved using an inexpensive banded solver, in a similar way to that of Maa et al. (1997), with the main difference that the present scheme involves 49 diagonals instead of 5. To conserve computer memory, the spare matrix is stored in two matrices; one contains the complex coefficients and the other contains the locations of each unknown. The solver constructs a small-banded matrix equation and then, follows the standard Gaussian elimination method with partial pivoting for forward elimination. Intermediate results are saved on the hard disk, and information is transferred between the two matrices during the procedure. This continues until the entire banded matrix equation is processed. Back substitution begins by reading the last saved data entry, one block at a time, and repeated until all saved blocks have been read and processed. Maa et al. (2002) have demonstrated the efficiency of this procedure.

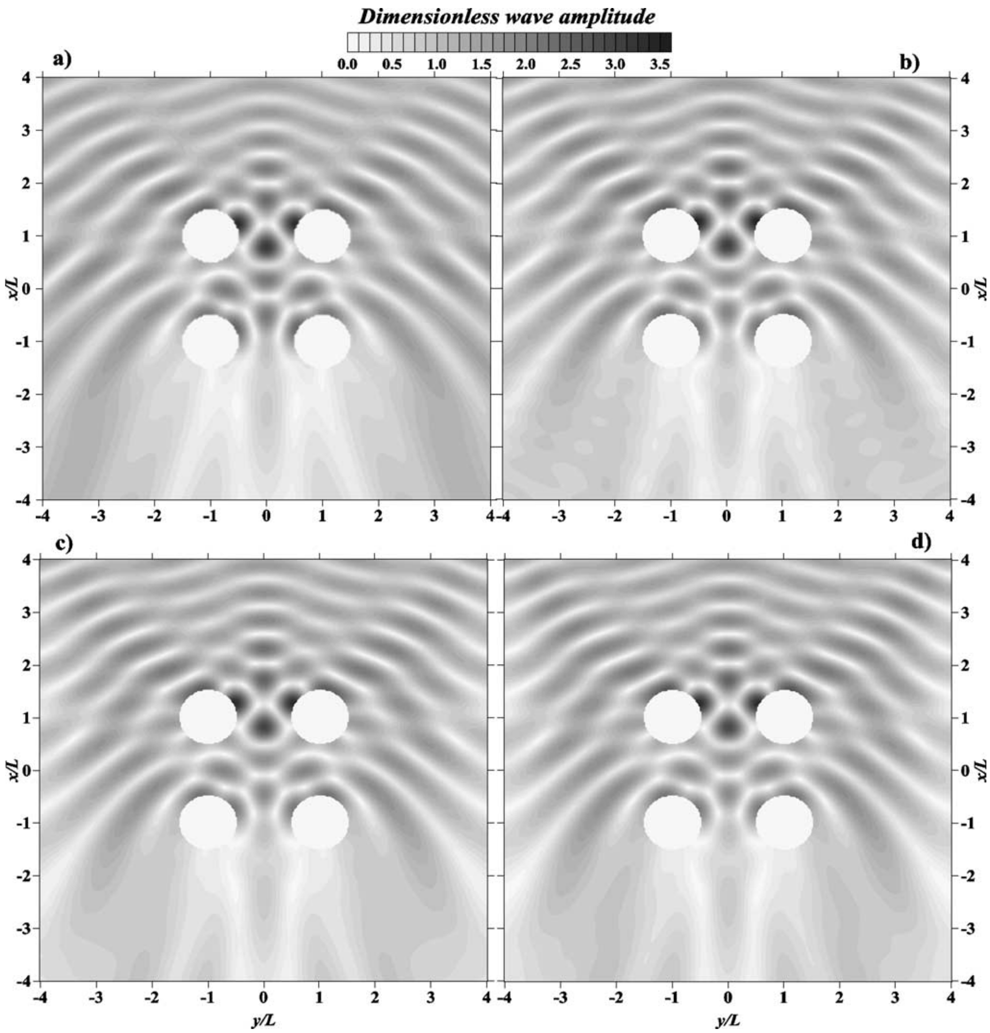

Fig. 2. Total dimensionless wave amplitude distribution: (a) analytical result; (b) Kirby (1986); (c) Padé approximation; (d) lowest parabolic approximation (kh=2π, θ=0°).

4. Results

The model is validated for the case of interaction of a monochromatic wave train with a group of four vertical surface-piercing cylinders located on a horizontal bed. Linton and Evans (1990) present an analytical solution for this problem. Each cylinder has radius, $r=L/2$, where L is the wavelength of the incident waves. In plan, the centres of the cylinders are located at the vertices of a square of side dimension equal to $2L$. The origin of the global horizontal Cartesian coordinate system is at the geometric centre of the array, with x and y as defined in Fig. 1. The undisturbed relative water depth is everywhere set to $kh=2\pi$.

Analytical and numerically predicted total dimensionless wave amplitude fields (combined incident and scattered fields) have been obtained for normally incident waves where $\theta=0°$. Fig. 2a presents the results using Linton and Evans analytical solution. Fig. 2b–d show the numerical results obtained on a square grid of resolution $\Delta x=\Delta y=L/40$, for different boundary approximation parameters. The results in Fig. 2b correspond to the parameter values derived by Kirby (1986) for maximum directional aperture (MDA) equal to 70° whereby $a_0=0.994733030$, $a_1=0.890064831$ and $a_2=0.451640568$. Fig. 2c is obtained using the Padé approximant [1/1] (PA) values: $a_0=1$; $a_1=0.75$ and $a_2=0.25$. Fig. 2d gives the wave amplitude field when the lowest parabolic approximation (LPA) is used, such that $a_0=1$, $a_1=0.5$ and $a_2=0$. This last set of parameters corresponds to the model presented by Maa et al. (2002). Although the structure of the scattered wave field in this case is complicated, it is clear that all the numerical predictions are in close agreement with the analytical solution. However, there are certain discrepancies. The predictions based on the parameter values associated with an MDA equal to 70° are affected by a small amount of artificial reflection at the external boundaries. The results obtained with the PA and the LPA parameter values have energy damping near the external boundaries. Fig. 3 plots the dimensionless wave amplitude profiles along the longitudinal $x/L=0$ and transverse $y/L=0$ lines that pass through the centre of the general coordinate system. The numerically predicted profiles obtained using the parameter values corresponding to an MDA equal to 70° are slightly closer to the analytical profiles than the predictions based on the PA parameter values, and significantly closer than the profiles for the LPA parameter values. For this reason, the parameter values for the following examples are set to those for an MDA equal to 70°.

Figs. 4 and 5 illustrate the total dimensionless wave amplitude distribution for waves that are obliquely incident to the cylinder array at an angle of $\theta=30°$. The equivalent results for an incident wave angle of $\theta=45°$ are given in Figs. 6 and 7. In both cases, the numerical predictions and analytical solution are in excellent agreement. Almost no effect is

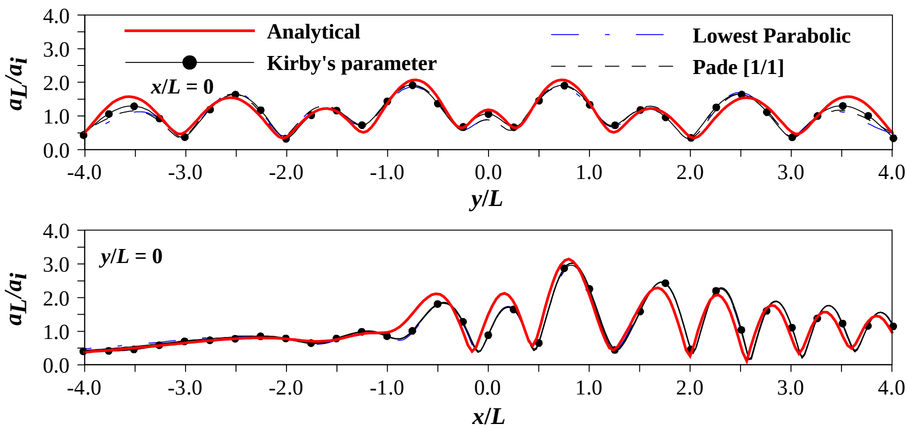

Fig. 3. Total dimensionless wave amplitude along $x/L=0$ and $y/L=0$ ($kh=2\pi$, $\theta=0°$).

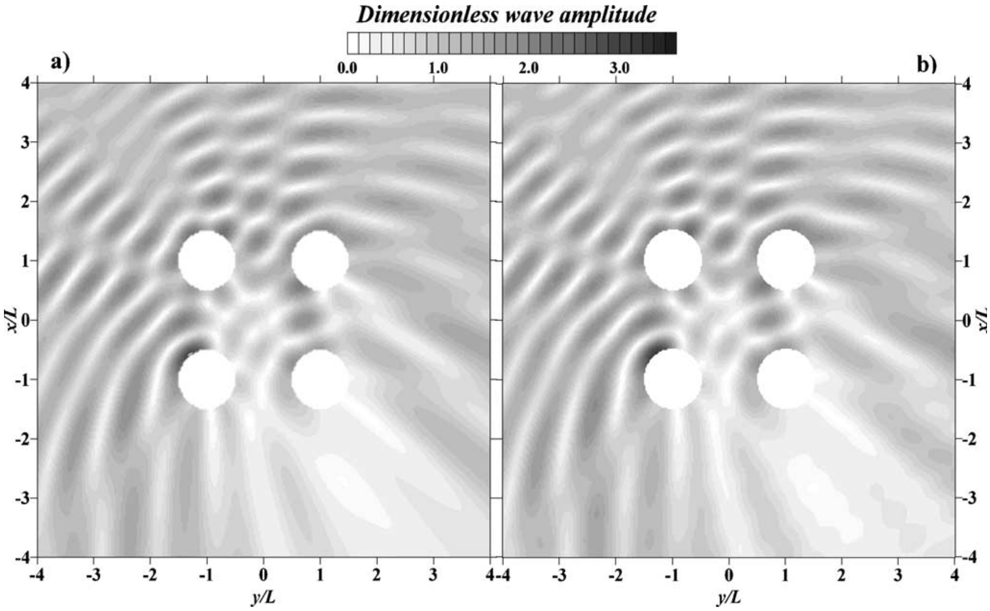

Fig. 4. Total dimensionless wave amplitude distribution: (a) analytical solution and (b) numerical model ($kh=2\pi$, $\theta=30°$).

discernible from artificial reflections at the external boundaries of the domain.

Next, the interaction of a monochromatic wave train with a square array of four cylinders each of radius $r=L/4$ in a relative water depth of $kh=\pi$ is considered in order to study the performance of the model for a case of longer relative wavelength. The cylinders are again located at the vertices of a square, with their centres spaced a distance L apart. Fig. 8 shows the total dimensionless wave amplitude for incident waves of direction $\theta=0°$. As in Fig. 2b, the results are influenced by noise generated by artificial reflections of the scattered waves at the open boundaries. The profiles in Fig. 9 indicated that the noise is at a very low level compared with the local wave amplitude.

The open boundary conditions used here are parabolic approximations to the mathematically elliptic boundary conditions. From the analysis carried out by Dingemans (1997), it can be deduced that use of parameter values proposed by Kirby (1986) for the parabolic approximation will always induce noise in

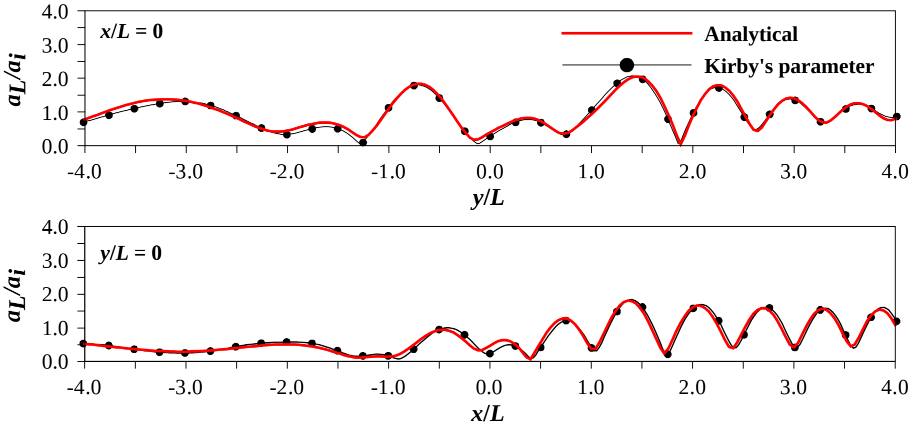

Fig. 5. Total dimensionless wave amplitude along $x/L=0$ and $y/L=0$ ($kh=2\pi$, $\theta=30°$).

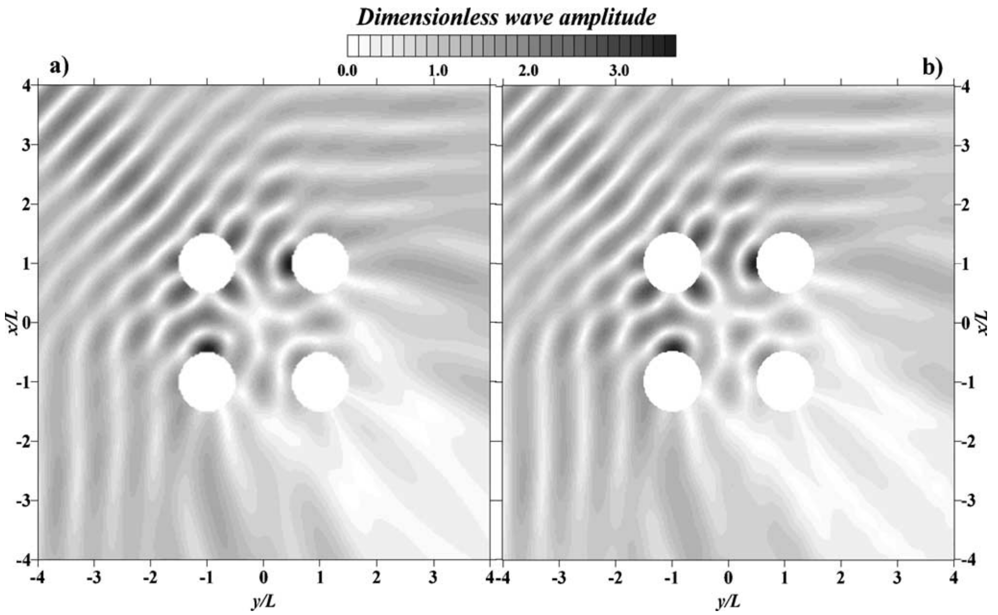

Fig. 6. Total dimensionless wave amplitude distribution: (a) analytical solution and (b) numerical model ($kh=\pi$, $\theta=45°$).

the wave amplitude field. However, this noise has a relatively small influence on the results presented above. Moreover, the discrepancies between the analytical and numerical results are partly due to the Cartesian stepped approximation to the curvature of the cylinder walls, as well as numerical errors inherent in the finite difference scheme.

With the development of offshore renewable energy devices such as wind turbines, it is likely that arrays of vertical surface-piercing cylindrical structures will be sited in shallow coastal waters. The wave-structure interaction simulations undertaken using the present model are therefore extended to consider cases where the cylinder array is mounted in shallow waters with uniform and non-uniform local bed topographies. Here, an array of four cylinders each of radius $r=L/4$ is configured so that the cylinder centres coincide with the vertices of a square of side length L. In the absence of local bed non-uniformity, the relative water depth is $kh=\pi/5$. The incident wave direction is $\theta=0°$. Fig. 10a presents the predicted total dimensionless

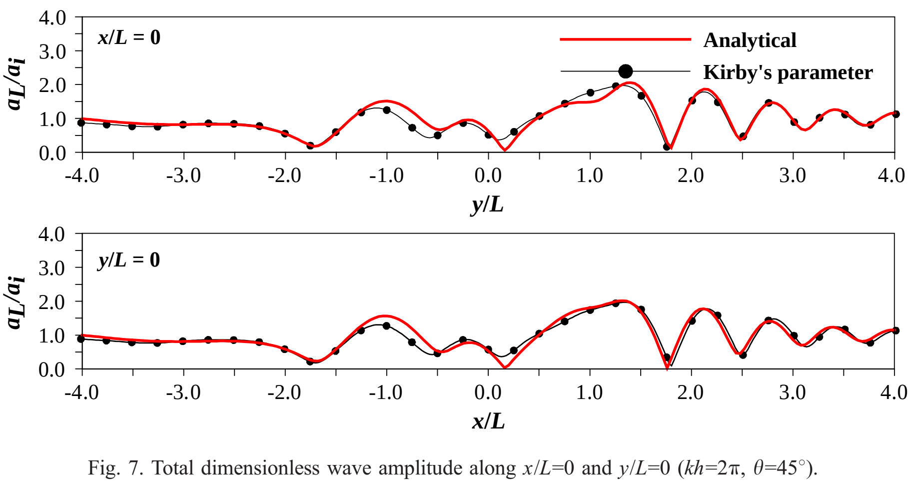

Fig. 7. Total dimensionless wave amplitude along $x/L=0$ and $y/L=0$ ($kh=2\pi$, $\theta=45°$).

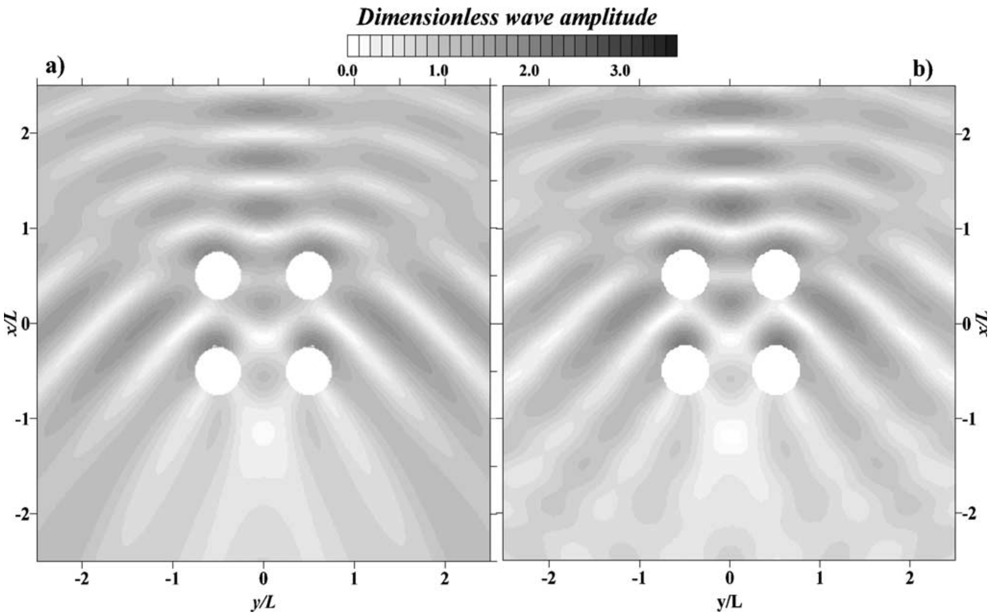

Fig. 8. Total dimensionless wave amplitude distribution: (a) analytical solution and (b) numerical model ($kh=\pi$, $\theta=0°$).

wave amplitude field for the case when the bed is everywhere horizontal. Fig. 10b and c show the equivalent results for cases where the otherwise horizontal bed contains a circular hump and a scour hole, respectively, where the non-uniform change to the bed elevation is $\delta=D(1-r/L)$ for $r\leq L$. The effect of undulating beds is shown in Fig. 10d and e, where the deviations of the bed to the horizontal are given by $\delta=D\sin(4\pi x/L)$ and $\delta=D\cos(4\pi x/L)$, respectively. Fig. 10f gives results for the horizontal bed over a distance of $3L$ followed by a plane beach of slope 0.1. In this last case, the incident wave amplitude of 1 m and dissipation induced by breaking were considered. In all cases D was chosen to be equal to 2 m. From Fig. 10 it is evident that the wave pattern is strongly dependent on the bed topography, which partly determines where minimum and maximum wave amplitudes

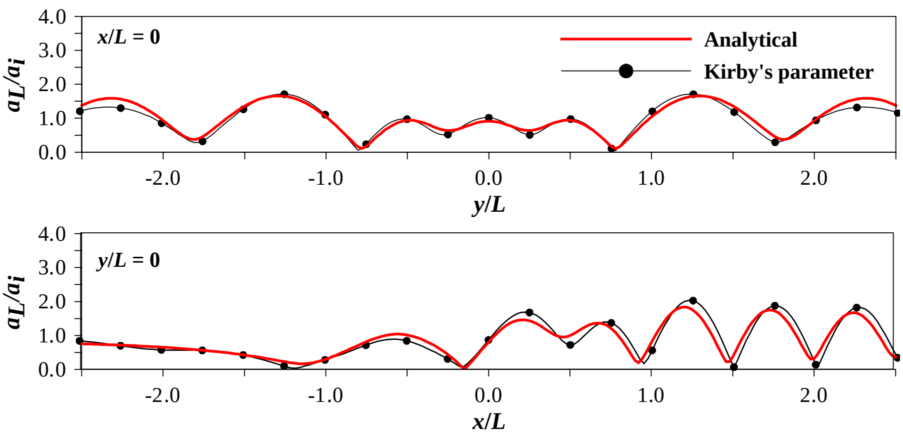

Fig. 9. Total dimensionless wave amplitude along $x/L=0$ and $y/L=0$ ($kh=\pi$, $\theta=0°$).

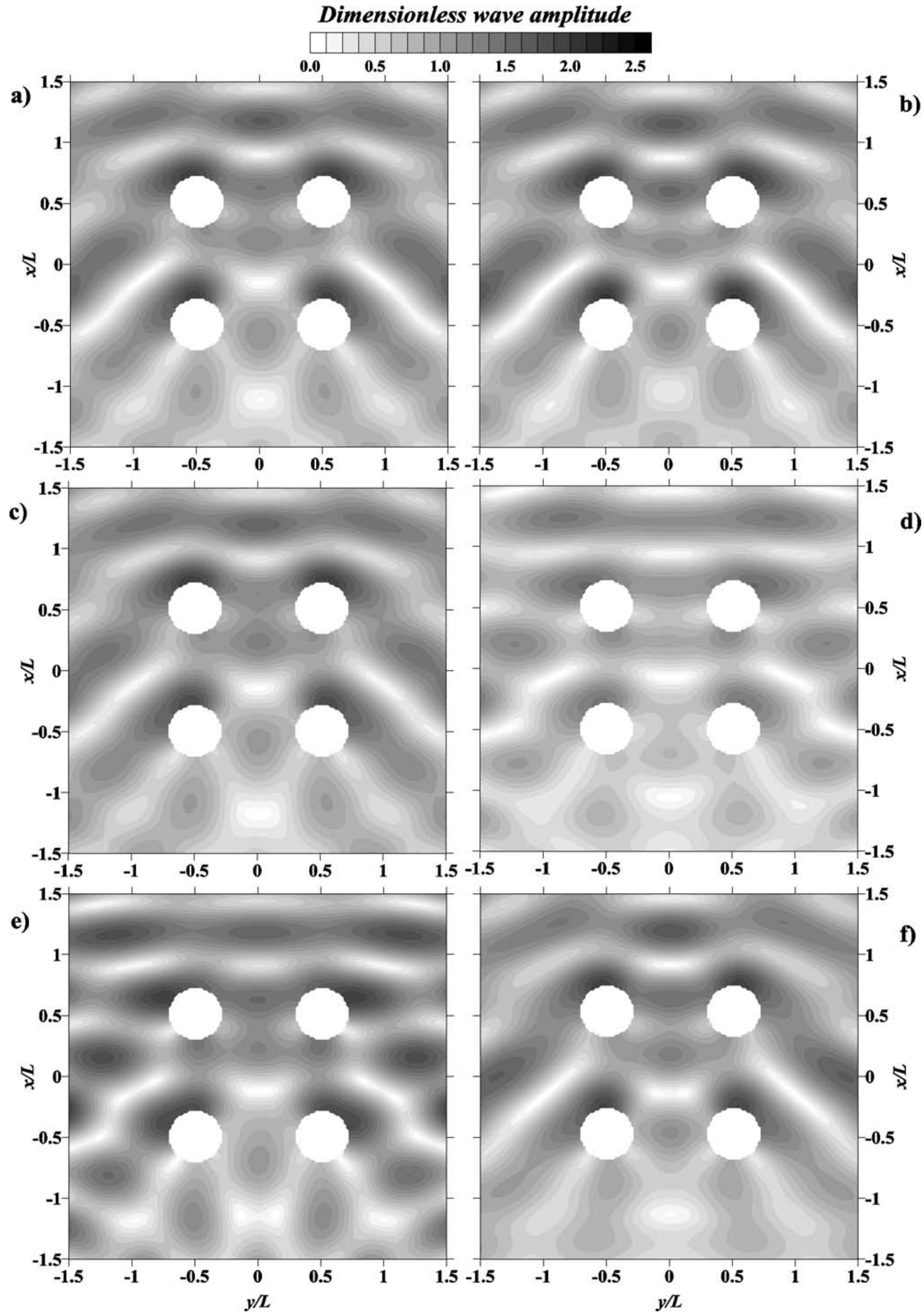

Fig. 10. Total dimensionless wave amplitude distribution: (a) horizontal bottom; (b) hump; (c) hole; (d) sinusoidal undulation; (e) cosinusoidal undulation; (f) in front of plane beach.

occur. Taking the results for the horizontal bed as reference values, the presence of the hump inside the four-cylinder array causes wave energy to concentrate in front of and between the two seaward cylinders and in the area surrounding the cylinder array. The presence of the scour hole produces less energy concentration. From Fig. 10d and e, it would appear that an undulated bed could cause considerable concentration or damping of wave energy. It is reasonable to anticipate that local wave energy focusing or damping would depend on the relative magnitude and phase of the bed undulations and incident wavelength. Wave reflections at other cylinders in the array structures and at the beach obviously also influence the wave energy distribution, as can be seen in Fig. 10f. The dimensionless wave amplitude profiles along the $y/L=0$ line, shown in Fig. 11, contain nodes close to $x/L=-1.2$, -0.2, 0.9 and 1.45 in all cases, and have similar overall behaviour. The largest discrepancies occur at the local wave maxima, where the variation in dimensionless wave amplitude exceeds 50% for the sinusoidally undulating bed.

In order to study the performance of the model for a case of a very large domain, the interaction of a monochromatic wave train with a rectangular array of 46 cylinders (23×2) each of radius $r=L/2$ in a relative water depth of $kh=0.4\pi$ is considered. The cylinders are located at the sides of a rectangle, with their centres spaced a distance $(4.5)^{1/2}$ L apart in the x- and y-directions. The analytical and numerically predicted dimensionless wave amplitude fields have been obtained for waves that are obliquely incident to the cylinder array at an angle of $\theta=45°$. The numerical grid covers an area of $52L\times 8L$ of resolution $\Delta x=\Delta y=L/50$ (2601×401 nodes). Fig. 12(a) and (b) present the analytical and numerically predicted total dimensionless wave amplitude fields using Linton and Evans (1990) solution and the MDA approximation, respectively. Fig. 12(c) shows the equivalent results for the case where an undulating bed was superimposed on the horizontal bed. The deviation of the bed from the horizontal is given by $\delta=D\sin(4\pi x/L)$ with $D=5$ m. Fig. 12(d) plots the total dimensionless wave amplitude profiles along the longitudinal $y/L=4$ line that passes through the centre of the general coordinate system. In this case, the numerical predictions and analytical solution are in excellent agreement. From this figure it is clear that the wave pattern is strongly dependent on the bed topography. Furthermore, with this example it has been shown that using double precision in the program code, the round-off error is negligible for solving a large banded matrix with up to 10^6 unknown variables. Based on a 2.8-GHz Pentium-IV PC with 1 GB of RAM memory and running the Windows XP operating system, the computing time (in seconds) necessary to solve the banded matrix is

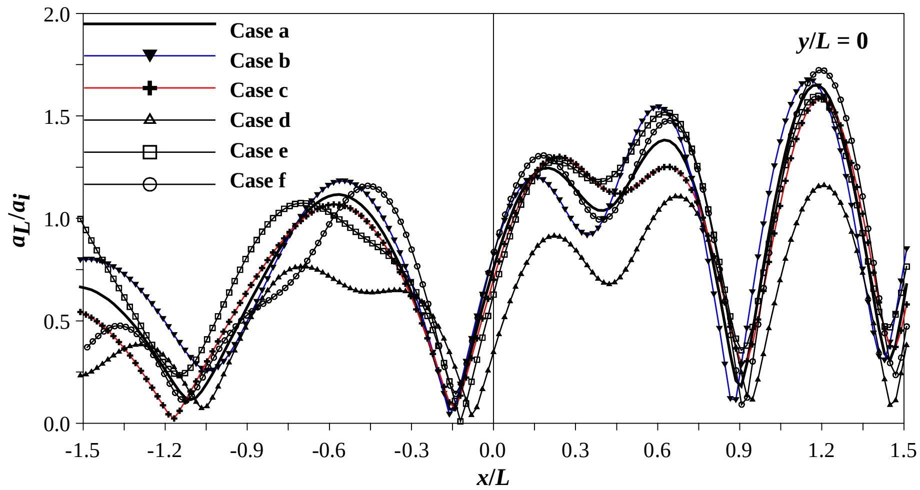

Fig. 11. Total dimensionless wave amplitude along $y/L=0$ for different sea bottom configurations.

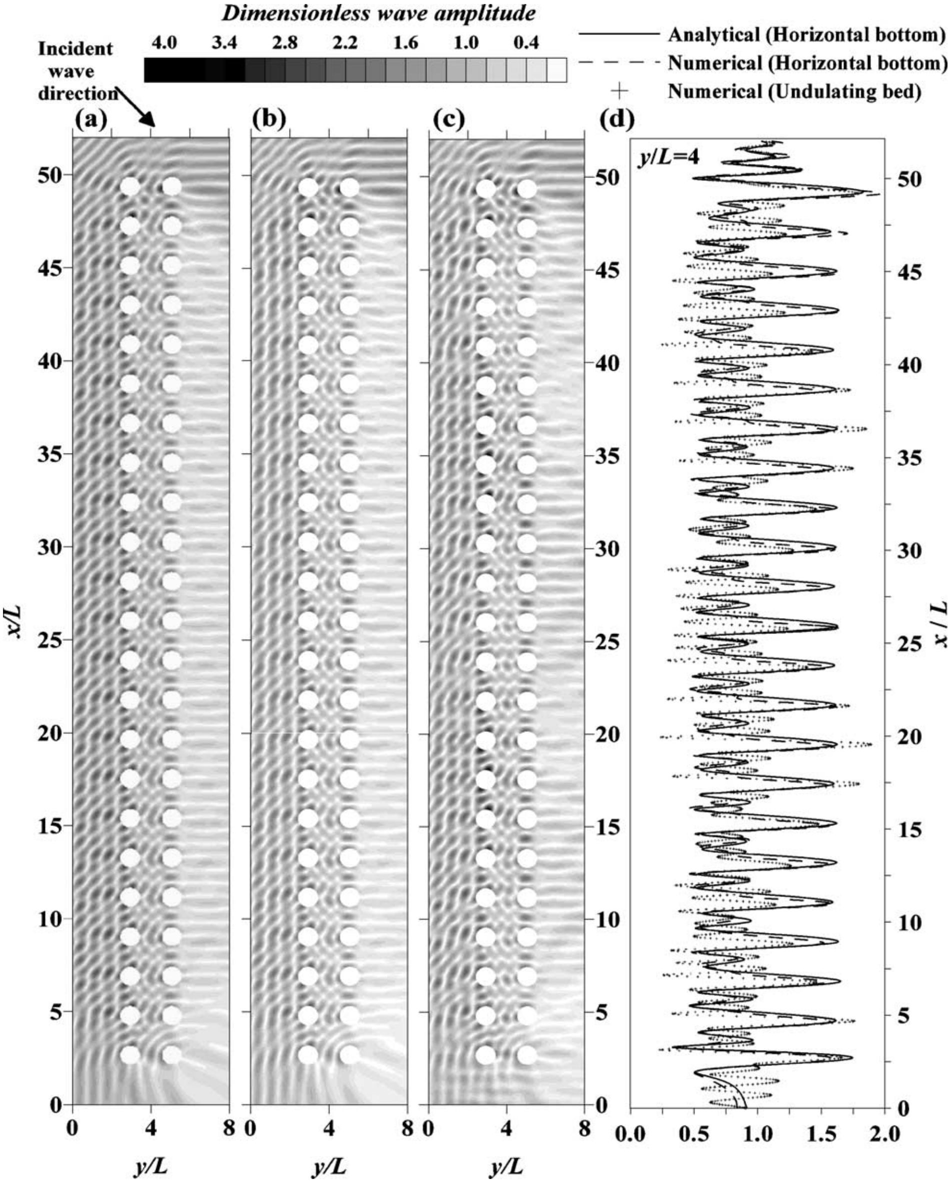

Fig. 12. Total dimensionless wave amplitude distribution: (a) analytical result (horizontal bottom); (b) MDA approximation (horizontal bottom); (c) MDA approximation (undulating bed); (d) dimensionless wave amplitude along y/L=4 (kh=0.4π, θ=45°).

approximately equal to $a_1 X_1 X_2^m$, where $a_1 = 4 \times 10^{-6}$, X_1=max(NX,NY), X_2=min(NX,NY) and m=2.8. For this example, the computing time required was almost 5.5 h.

Xu and Panchang (1993) and Chamberlain and Porter (1999) considered wave scattering by a circular island using a direct numerical approach to approximate the mild-slope and the modified mild-slope equations. The island is of radius r_a=10 km with a shoal in the form $h(r)$=ár^2 (with $\alpha = hb/r_b$). At horizontal distances greater than r_b=30 km from the centre of the island, the depth is constant and equal to hb=4 m. The grid resolution used for the numerical results was $\Delta x = \Delta y = r_b/40$. Fig. 13 presents results for regular waves of period 240 s. The left-hand side of Fig. 13 shows the total dimensionless wave amplitude

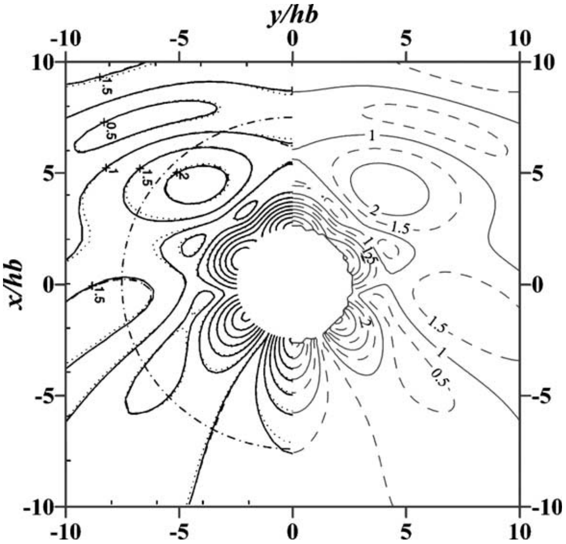

Fig. 13. Total dimensionless wave amplitude amplification factors. Left-hand side, Chamberlain and Porter (1999); right-hand side, present model.

results reported by Chamberlain and Porter (1999), and the right-hand side shows predictions obtained with the MDA approximation. The MDA approximation results are in very close agreement with those of Chamberlain and Porter (1999).

5. Conclusions

A second-order accurate central difference scheme has been described for solving the modified time-independent mild-slope equation with an energy dissipation term. Special attention has been paid to the treatment of open and reflecting boundary conditions by means of a second-order parabolic approximation. An efficient direct solver has been implemented for the discretised equations, which form a sparse banded matrix with 49 diagonals. The direct solver is essentially an extension of the method applied by Maa et al. (1997) to a sparse banded matrix with 5 diagonals.

Numerical predictions of the wave amplitude field are in close agreement with the analytical solution of Linton and Evans (1990) for the interaction of non-breaking regular waves with an array of vertical surface-piercing circular cylinders on a horizontal sea bed. Slight differences between the analytical and the numerical model results are due to the stepped approximation of the circular boundary of the cylinders as well as numerical errors in the finite difference scheme. Parameter values for the parabolic approximation to the elliptic radiation boundary condition have been investigated. Values based on a maximum directional aperture of 70° (Kirby, 1986) give more accurate results than those based on the Padé approximant [1/1]. Although the MDA approach induces spurious reflections or dissipation at the boundaries, the inaccuracies are of extremely small magnitude. This finding is in agreement with the conclusions presented by Kirby (1989).

Further model tests for non-uniform bed topographies including a hump, a scour hole and bed undulations indicate that wave energy focusing or damping can be greatly affected by the local bathymetry in shallow coastal waters. This is obviously important in the design of array-type coastal structures, such as offshore wind farms.

The model is robust, and applicable to wave propagation in cases involving complicated geometrical configurations. At the boundaries, the present model has fewer restrictions associated with wave obliqueness than other mild-slope equation models, and does not require absorbing sponge layers. The CPU time for a simulation involving 40,000 water cells takes about 40 min on an 800-MHz desktop PC.

Acknowledgements

This research was partially funded by the Mexican Consejo Nacional de Ciencia y Tecnología, CONACYT, project “Estabilidad e Influencia de estructuras marinas sobre el litoral” under contract J 37157-U.

References

Berkhoff, J.C.W., 1972. Computation of combined refraction diffraction. Proc. 13th Intl. Conf. on Coastal Engng. ASCE, Vancouver, Canada, pp. 471–490.

Booij, N., 1983. A note on the accuracy of the mild slope equation. J. Fluid Mech., 291, 393–407.

Chamberlain, P.G., Porter, D., 1995. The modified mild slope equation. J. Fluid Mech., 291, 393–407.

Chamberlain, P.G., Porter, D., 1999. Scattering and near-trapping of water waves by axisymmetric topography. J. Fluid Mech., 388, 335–354.

Copeland, G.J.M., 1985. A practical alternative to the "mild-slope" wave equation. Coast. Eng., 9, 125–149.

Dally, W., Dean, R., Dalrymple, R., 1985. Wave height variation across beaches of arbitrary profile. J. Geophys. Res., 90 (C6), 11917–11927.

Dingemans, M., 1997. Water wave propagation over uneven bottoms. Advanced Series on Ocean Engineering, vol. 13. World Scientific, Singapore.

Kirby, J.T., 1986. Rational approximation in the parabolic equation for water waves. Coast. Eng., 10, 355–378.

Kirby, J.T., 1989. A note on parabolic radiation boundary conditions for elliptic wave calculations. Coast. Eng., 13, 211–218.

Kirby, J.T., Dalrymple, R.A., 1994. Combined Refraction/Diffraction Model REF/DIF 1, Version 2.5. Documentation and User's Manual, Research Report No. CACR-94-22. Center for Applied Coastal Research, Department of Civil Engineering, University of Delaware, Newark, USA.

Linton, C., Evans, D., 1990. The interaction of waves with arrays of vertical circular cylinders. J. Fluid Mech., 215, 549–569.

Maa, J. P.-Y., Maa, M.-H., Li, C., He, Q. 1997. Using the Gaussian Elimination Method for Large Banded Matrix Equations, Special Scientific Report, No. 135, Virginia Institute of Marine Science, Gloucester Point, VA 23062.

Maa, J.P.-Y., Hsu, T.-W., Lee, D.-Y., 2002. The RIDE model: an enhanced computer program for wave transformation. Ocean Eng., 29, 1441–1458.

Madsen, P.A., Larsen, J., 1987. An efficient finite-difference approach to the mild-slope equation. Coast. Eng., 11, 329–351.

Massel, S.R., 1993. Extended refraction–diffraction equation for waves over rippled beds. J. Fluid Mech., 162, 171–186.

Oliveira, F.S.B.F., Anastasiou, K., 1998. An efficient computational model for water wave propagation in coastal regions. Appl. Ocean Res., 20, 263–271.

Panchang, V.G., Ge, W., Cushman-Rosin, B., Pearce, B.R., 1991. Solution to the mild slope wave problem by iteration. Appl. Ocean Res., 13 (4), 187–199.

Porter, D., Staziker, D., 1995. Extension of the mild-slope equation. J. Fluid Mech., 300, 367–382.

Radder, A.C., 1979. On the parabolic equation method for water wave propagation. J. Fluid Mech., 95 (1), 159–176.

Smith, R., Sprinks, T., 1975. Scattering of surface waves by a conical island. J. Fluid Mech., 72, 373–384.

Steward, R.D., Panchang, V.G., 2000. Improved coastal boundary condition for surface waves. Ocean Eng., 28, 139–157.

Suh, K.D., Lee, C., Park, W.S., 1997. Time-dependent equations for wave propagation on rapidly varying topography. Coast. Eng., 32, 91–117.

Xu, B., Panchang, V., 1993. Outgoing boundary conditions for finite-difference elliptic water-wave models. Proc. R. Soc. Lond., A, 441, 575–588.

Zhao, L., Panchang, V., Chen, W., Demirbilek, Z., Chhabbra, N., 2001. Simulation of wave breaking effects in two-dimensional elliptic harbor wave models. Coast. Eng., 42, 359–373.